IEEE Access
Multidisciplinary | Rapid Review | Open Access Journal

Received 15 October 2023, accepted 2 November 2023, date of publication 6 November 2023,
date of current version 10 November 2023.

Digital Object Identifier 10.1109/ACCESS.2023.3330243

RESEARCH ARTICLE

A Highly Integrated Radio Frequency Receiver RF CMOS Module for Core Body Temperature Thermometer

IKHWAN KIM[1], WONIL JANG[1,2], HYEON-SIK HWANG[1,2], BYEONG-JAE SEO[1,2], DONG-MIN LEE[1], JI-HO HAN[3], JAE-WOO SHIN[3], YOUNG-RO YOON[3], TAEHYOUN OH[1], HYUNG-CHUL PARK[4], EUN-SEONG KIM[1], YUN-SEONG EO[1,2], (Member, IEEE), AND NAM-YOUNG KIM[1]

[1]RFIC Center, Kwangwoon University, Seoul 01897, Republic of Korea
[2]Silicon Research and Development Company Ltd., Bundang-gu, Seongnam 13510, Republic of Korea
[3]Easytem Company Ltd., Geumcheon-gu, Seoul 08594, Republic of Korea
[4]Department of Electronic and IT Media Engineering, Seoul National University of Science and Technology, Seoul 01811, Republic of Korea

Corresponding authors: Yun-Seong Eo (yseo71@kw.ac.kr) and Nam-Young Kim (nykim@kw.ac.kr)

This work was supported in part by the ATC+ (Advanced Technology Center plus) Program through the Korea Evaluation Institute of Industrial Technology under Grant 20017980, funded by the National Research Foundation of Korea (NRF) and the Korean government (MIST) under Grant RS-2023-00302751. It was also supported in part by Easytem Company Ltd.

ABSTRACT This paper presents a highly integrated radio frequency (RF) CMOS receiver module for monitoring the core body temperature thermometer, which operates in the dual band 1.35 and 2.75 GHz ranges. The RF receiver IC, such as a Dicke radiometer, includes the full receiver circuits, RF switch and modulator, and duty calibrating circuit using a 65 nm CMOS process. With the proposed duty cycle modulation, accurate temperature sensing is achievable even with a receiver gain mismatch and fluctuation. The measured temperature ranges from 22 to 47.3°C, and the measured voltage slope is 2.97 mV/ms • °C, and the temperature error is less than 0.9°C in 1.35 GHz band. The radiometric RF CMOS IC has a size of 1.6×2.3 mm^2 and the current consumption of 52 mW. Unlike the general skin temperature measurement of existing infrared (IR) sensors, the RF microwave core body thermometer equipped with an RF receiver IC that measures core body temperature inside a human body will be used in various fields as a digital healthcare and medical device.

INDEX TERMS Dicke radiometer, total power radiometer, temperature sensor IC, duty cycle modulator, RF CMOS.

I. INTRODUCTION

Plank's law describes the spectral power density of the electromagnetic radiation emitted by an object as a function of its temperature and the frequency [1]. The Rayleigh-Jeans approximation describes the linear relationship between the radiated spectral power and temperature, enabling us to measure the temperature using a microwave radiometer by measuring the power radiated from an object.

In this day, most people try to use invasive methods to measure deep core temperature. However, invasive methods can cause damage to human tissues [2], [3].

To minimize this damage, the use of non-invasive methods for measuring human deep core temperature with a microwave radiometer has been studied [4], [5], [6]. In our early studies on measuring deep core temperature with microwaves, we designed a microwave antenna for this purpose, provided a brief explanation of the background theory related to measuring deep core temperature, and presented the radiometer block diagram [7], [8].

Most of the early literature illustrate radiometers implemented with many discrete monolithic microwave integrated circuit (MMIC) components. As a result, the overall module becomes bulky and the power consumption is high [9], [10], [11]. A few studies have attempted to address the size problem of integrated chip (IC) based radiometers [12], [13],

The associate editor coordinating the review of this manuscript and approving it for publication was Fabian Khateb.

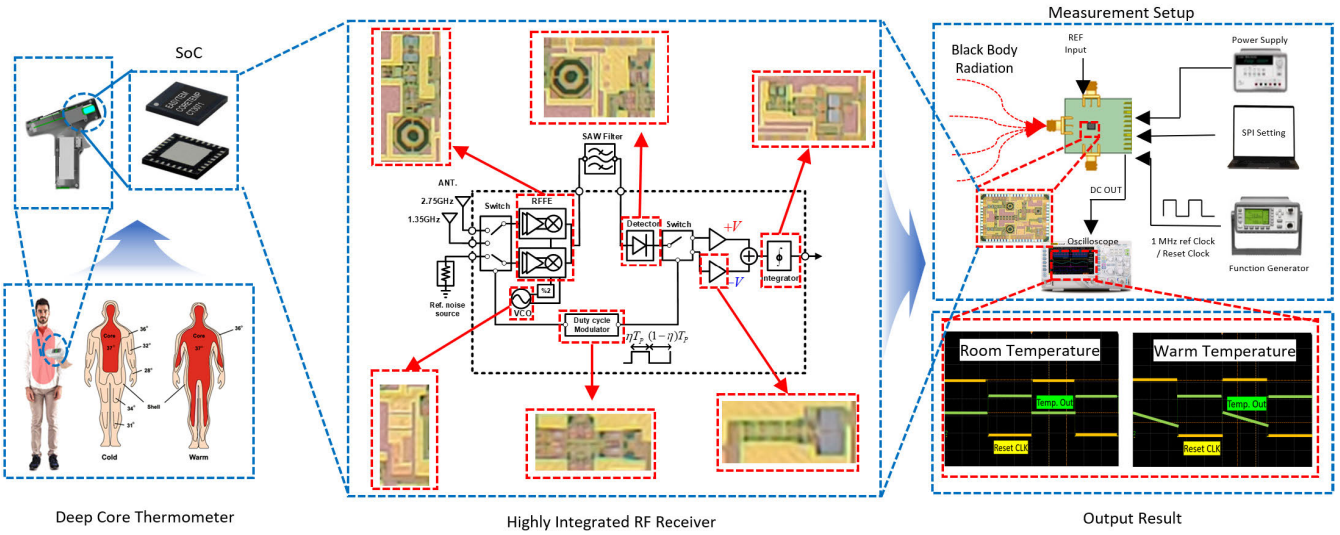

FIGURE 1. A highly integrated radio frequency receiver module for core body temperature monitoring system.

[14], [15], [16]. However, all of them deal with partially integrated radiometers, which contain many external components high power consumption. To reduce the temperature error considerably, the Dicke radiometer [17], whose gain error is calibrated, must be employed instead of a total power radiometer (TPR) [19], [20]. To the best of the authors' knowledge, this study presents the first Dicke radiometer system-on-chip (SoC) for measuring core body temperature that includes the full RF receiver blocks except IF SAW filter. The band limited noise powers of the antenna and reference temperature source are amplified and detected alternatively via the receiver. By controlling the duty cycle of the switching clock, the time varying gain error between two different paths can be calibrated and greatly reduced. Since the measured output voltage of the Dicke radiometer is proportional to the temperature difference rather than to the absolute temperature, the accuracy is fairly good compared with that of a total power radiometer. Moreover, since the receiver SoC eliminates most of the external components while consuming little power, the radiometer can achieve the features of low power and small size using the Dicke receiver IC.

To choose the proper frequency band for the lower microwave interferences [21], the dual band receiver is designed for 1.35 GHz and 2.75 GHz. These bands are scarcely utilized by communication standards, and it has few spurious signals. The band for better performance can be selected while measuring the temperature with respect to the temperature measurement stability and accuracy.

The signal from the human deep core is weak and challenging to receive with a microwave radiometer. Therefore, choosing a frequency band with minimal microwave interference is crucial. One of the main reasons our proposed radiometer has a dual-band configuration is to minimize the possibility of receiving unwanted signals and to ensure global compatibility. To the best of our knowledge, the 1350 MHz and 2750 MHz bands have only a few instances of microwave interference in South Korea. However, there is a possibility that one of these bands may be restricted or widely used in some countries. Nevertheless, our proposed radiometer is dual-band, so even if one of the bands cannot be used, the other band can still be employed to measure deep core temperature. Fig. 1 shows the proposed Dicke radiometer for measuring core body temperature. The receiver die is fabricated using a 65 nm complementary metal-oxide semiconductor (CMOS) technology. Therefore, the highly integrated Dicke radiometer SoC can provide the key solution to realize light and battery-powered non-invasive temperature sensors for various temperature monitoring applications.

II. MICROWAVE RADIOMETER ARCHITECTRUE AND CIRCUITS

A. DICKE RADIOMETER ARCHITECTURE

The proposed dual-band Dicke radiometer employs the conventional heterodyne receiver architecture as shown in Fig. 2. The RF input port for each band (1.35/2.75 GHz) is separated, and the following analog circuit blocks after the down conversion mixer are shared for both bands. The radiometer receiver includes all the circuit blocks for noise power detection namely the RF front end amplifier stages, mixer, local oscillation (LO) generation block, intermediate frequency (IF) stage power detector, integrator, clock modulation block, and calibration blocks on a single die. Since all the circuit blocks for the Dicke radiometer are integrated on a single die, a small sized SoC-based radiometer sensor can be realized compared with the previously reported modular-form sensors, which employs many discrete MMICs and analog components.

The noise power bandwidth is determined by the external IF surface acoustic wave (SAW) filter bandwidth. The noise signals from the antenna and reference sources are amplified

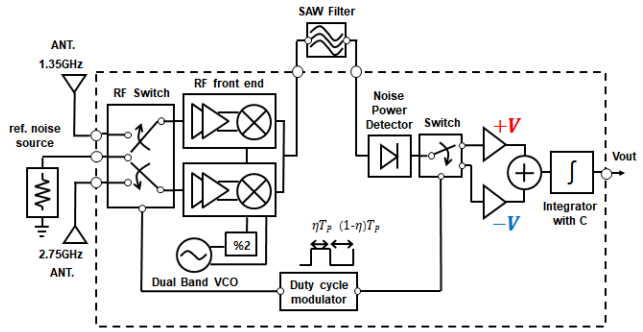

FIGURE 2. Proposed dicke radiometer block diagram.

and filtered in the RF front end circuit, and then converted to a DC voltage that is proportional to the noise power at the detector input. To confine the noise power bandwidth with the strict requirement, an IF SAW filter (RF3608D), whose center frequency and 1 dB bandwidth are 426 MHz and 19.5 MHz respectively, is used in the IF stage. Since the measured RF noise bands are approximately 1.35 GHz and 2.75 GHz, respectively, the desired LO frequencies for the down-conversion are approximately 924 MHz and 2324 MHz, respectively, which is generated by a single CMOS voltage-controlled oscillator (VCO) and frequency divider. The dual band LO generator circuit is composed of the VCO core, switched divider, and buffer amplifiers, which enables proper RF band selection to minimize the in-band interferers.

Compared with the conventional TPR receiver, the Dicke radiometer has two switched noise power receiving paths and achieves precise temperature measurement by using the power difference rather than the absolute noise power [16].

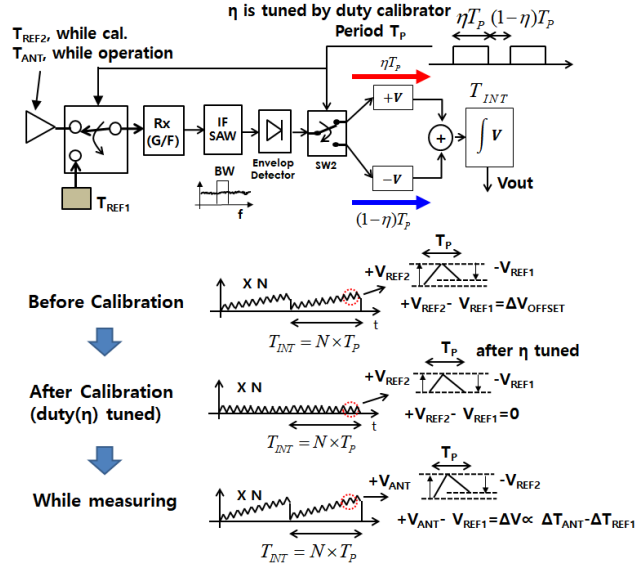

FIGURE 3. Calibration and temperature measurement procedure.

The procedure of achieving pre-calibration and actual measurement is illustrated in Fig. 3. During the initial calibration step, the antenna port is connected to reference 2 (TREF2) and the noise power of reference 2 is received and detected in the receiver during the ηTP duty, where the duty cycle modulator generates a switching clock of period TP and variable duty cycle η. In the next interval of $(1-\eta)$TP, the RF switch is changed and the noise power from reference 1 (TREF1) is fed to the receiver and measured at the output of the integrator. Since the receiver voltage gain for each path has the opposite sign, the voltage integrated during the full period TP is VREF2 (the output of the integrator while reference 2 is connected.) subtracted by VREF1 (while reference 1 is connected.). For a 50 % duty cycle, the gain mismatch or gain drift between two paths causes a non-zero voltage (ΔVOFFSET) at the output of the integrator. Since the switched integration is repeated N times to achieve a sufficient signal to noise ratio (SNR), the final integrated output voltage becomes N·ΔVOFFSET.

To compensate for the offset voltage, a clock-duty calibrator adjusts the duty cycle deliberately such that the integrator output could become zero after the calibration as shown in Fig. 3. Following the calibration procedure, the temperature measurement of the target is performed by measuring the noise power originating from the antenna port.

B. DICKE RADIOMETER CIRCUIT DESIGN

As shown in Fig. 2, the designed radiometer is composed of a Dicke switch, low noise amplifier (LNA), Mixer, LO generation circuit, envelope detector, switching modulator, and integrator. The off-chip IF SAW filter component is used for the noise bandwidth definition.

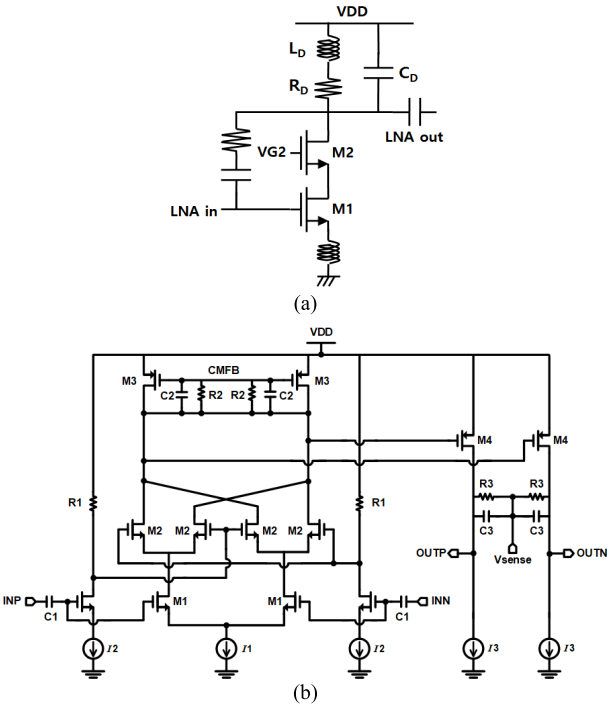

FIGURE 4. Calibration and temperature measurement procedure (a) LNA and (b) power envelope detector.

Fig. 4 (a) shows the single-band LNA circuit adopting an inductive source degenerated cascade amplifier with resistive feedback, compromising between the noise figure and the bandwidth. The circuit topologies for both bands are similar, but each LNA is optimized independently according to the RF input allocated for each band. Following the LNA, a single to differential (S2D) amplifier is used for the differential fashion. The differential structure is robust against common mode noise generated by the power supply or the substrate, providing low noise receiver performance. The down conversion mixer is a Gilbert cell-based active mixer that uses the current bleeding technique. Current bleeding was used to reduce the flicker noise of the MOSFET at the transconductance stage and expand the voltage headroom.

The RF noise power is down-converted, and the effective noise bandwidth is defined by the off-chip SAW filter in the IF stage. In the envelope detector shown in Fig. 4 (b), an output voltage that is linearly proportional to the power is provided at the output, which corresponds to the absolute temperature value. The output DC voltage of the envelope detector linearly increases with the input noise power, where the slope is 2.3 dBV/dBm. The envelope detector core is a self-mixing circuit that adopts the Gilbert cell mixer topology with the active load. The common mode voltage at the output nodes is sustained at VDD/2 using the common mode feedback circuit not shown in Fig. 4 (b). The IF-stage switch in the modulator changes the receiver path for each power measure of the antenna and reference source, and is synchronized with the RF switch. The integrator stage accumulates the measured voltage in a certain period to increase the integrator output to the desired level and the SNR is greatly enhanced for accurate measurement. The antenna to reference switching clock has a 1 μs period and the integration time is 1 or 10 ms to improve the SNR performance. Responsivity and noise equivalent power (NEP) of detector can be defined by following equation (1) and (2) where V_{out_DC} is out put DC voltage, P_{RF_in} is input RF power, and P_n is noise power spectral density.

$$R_d = V_{out\_DC}/P_{RF\_in} \tag{1}$$

$$NEP = P_n/R_d \tag{2}$$

The simulated results for detector responsivity and NEP are 5×10^{11} V and $1.75 \times 10^{-20} W/\sqrt{Hz}$, respectively, at -110 dBm of RF input when external LNA, RFFE, and IF gains of 20 dB, 30 dB, and 30 dB exist. The duty cycle modulator as shown in Fig. 5 generates a switching clock with the precisely tuned duty cycle for the RF switch and modulator. It consists of a variable inverter chain, digitally trimmed charge pump controller (CPC), and inverter bias generator. The CPC has 14 binary-scaled CMOS inverter cells, which provides the digitally tunable unbalanced current between the NMOS and PMOS cells. Of these, 10 bits are included in the coarse tuning block and the other 4 bits in the fine calibration block.

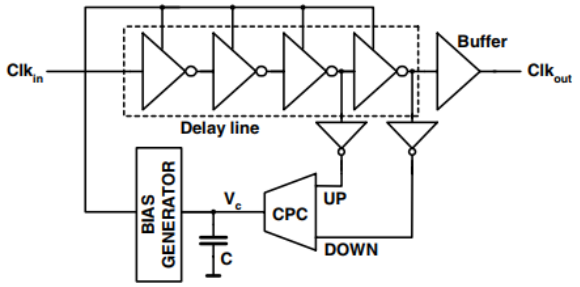

FIGURE 5. Circuit Schematic of duty cycle modulator.

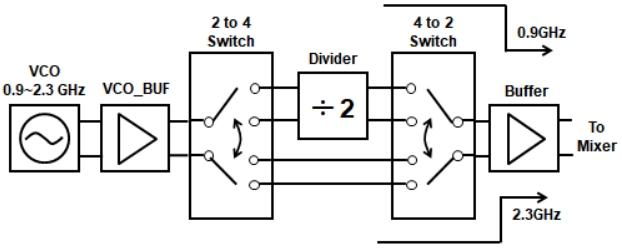

FIGURE 6. Block diagram of dual band LO generator.

The bias generator circuit that uses V_c provides two separate trimming voltages for NMOS and PMOS transistors in the inverter delay cell so that the duty cycle tuning the calibration can be performed. The simulated duty control scope ranges from 44.9 to 63.78 %, and the resolution of the duty control is about 0.0012 %/bit. The duty control circuit only consumes 640 μA at 1.2 V supply. Even though the duty is not linearly controlled by the duty control code, the monotonicity is approved in the simulation results. The simulated power consumption of the full receiver is 32.5 mW at 1.2 V supply.

The LO generation block is composed of a VCO, a switched frequency divider, and buffer amplifier, as illustrated in Fig. 6.

The VCO core is a CMOS cross coupled topology with the on-chip LC tank and the switched capacitor bank for the wide-band frequency tuning. For dual-band LO generation, the frequency range of the VCO is designed from 0.924 GHz to 2.324 GHz with a sufficient range margin. Frequency tuning can be performed with the analog tuned varactor and the digitally tuned capacitor bank. Since the receiver adopts the heterodyne architecture, the noise power is unaffected by the phase noise or slight frequency drift owing to the free-running VCO. The VCO frequency can be adjusted by using the switched capacitor combined with an LC resonator via SPI digital control. The LO generation for the lower band is $f_{VCO}/2$ signal provided by the frequency divider, and the direct VCO output is used for the higher band.

C. DICKE RADIOMETER CALIBRATION

The proposed calibration of the Dicke radiometer was performed with a Dicke switch, modulator, and duty-cycle modulator. Owing to the gain and noise figure (NF) mismatch

and fluctuation between the two receiver paths, a slight error occurs at the output and it can be eliminated with the calibration. By steering the RF switch and IF modulator periodically, the subtracted voltage output of the antenna noise power from the reference noise power can approach zero if the exact duty calibration is performed. Concerning the resolution of the duty-cycle control, the modeling and formulation of the Dick receiver states that

$$\Delta\eta \leq \frac{\Delta T_{REC}}{4T} \tag{3}$$

where $\Delta\eta$ denotes the duty calibration resolution, ΔT_{res} indicates the temperature accuracy, and T is the room temperature. Therefore, if we assume that T and ΔT_{res} are 300 K and 0.1 K respectively, $\Delta\eta$ should be less than 8.3×10-5. The tunable range of η is set to be 50 % and the digital duty controller resolution should be more than13 bits ($\sim$ 8,000). A 14-bit duty control scheme with coarse (10 bits) and fine (4 bits) modulators is applied, and $\Delta\eta$ is approximately 3.1×10^{-5}.

The calibration is performed using the following procedures. First, the antenna port is connected to a 50 Ω source that has the same temperature as the reference noise source. The reference noise source for calibration and measurement is implemented using a resistor for heating, temperature sensor IC, and feedback circuits for the temperature stabilization. The temperature of the reference source can be monitored with the temperature sensor IC output, and a bang-bang control method is employed to perform heating using the resistor. The integrator DC output reflects the mismatch and the fluctuation of the gain and NF between two receiver paths. By measuring the DC value and controlling the duty cycle digitally, the DC output can reach to zero value with sufficient accuracy. This is the end of the calibration. Subsequently, the reference source connected to the antenna port is replaced by the target noise source or antenna to measure the temperature of the target. The temperature difference between the reference temperature and the antenna or target can be calculated by measuring the accumulated DC output at the integrator output.

III. MEASUREMENT RESULTS

Fig. 7 shows the fabricated Dicke radiometer IC and the evaluation module implemented to verify its performance. The designed radiometer IC was fabricated using a 65-nm CMOS process. The size of the radiometer IC is 1.6 × 2.3 mm. An IF SAW filter of 19.5 MHz bandwidth is mounted on the back side of the PCB board. In this work, to evaluate the radiometer IC performance irrelevant to the antenna or environmental characteristics, two 50 Ω reference temperature source boards were prepared so that one could be used as the reference noise source and the other as a target or test noise source. The resistive heating circuit and temperature sensor are mounted on the board to measure and control the board temperature.

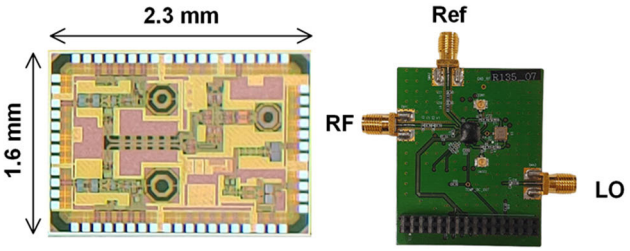

FIGURE 7. Dicke radiometer IC die photo and evaluation board.

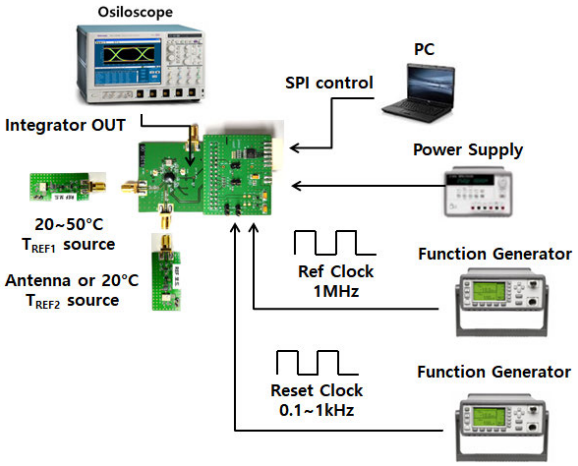

FIGURE 8. Test set environment for the dicke radiometer IC.

Fig. 8 illustrates the test environments of the calibration procedure and the measurement of the target temperature. A current driven heating resistor and a nearby temperature sensor IC are mounted closely on the reference temperature board. The heating current can be controlled by a variable resistor. By monitoring the temperature sensor and adjusting the resistor value, we can obtain the desired thermal noise source from the reference temperature board. Due to the accuracy of the sensor IC, the resolution of temperature control is around 0.5 °C.

Fig. 9 shows the simulated and measured gain and NF of the RF front-end part, from the LNA to the IF amplifier. The simulated and measured results do not exactly match, and this is because the simulated results show gain and NF without the SAW filter. On the other hand, the measured results show gain and NF with the SAW filter. The IF SAW filter (RF3608D) cannot be realized in simulation. As shown in Fig. 10, the measured gain and NF of the RF front-end part, from the LNA to the IF amplifier, are 37.8 dB and 3.2 dB, respectively, in the lower band.

In the higher band, the measured gain and NF are more than 23 dB and less than 7 dB, respectively. Moreover, the measured duty control ranges from 40.3 to 72.5 % with a 14-bit resolution, as shown in Fig. 10. Even though the linearity varies, the monotonicity is made sure to be maintained over the full range for the proper duty control.

TABLE 1. Comparison with the other radiometer performance.

Reference	Frequency band	Architecture	Temperature Range/ Temperature Accuracy	IC Integration	DC power	Application
[7]	1.4 GHz	Total Power	Room Temperature/ 0.5 K	Hybrid Module	N.A. (much power)	Body temperature Measurement
[8]	36.8 GHz	Dicke Radiometer	0 – 500 K/ 1K (design)	Hybrid Module	N.A. (much power)	Fire Detection
[9]	3.4 – 4.1 GHz	Dicke Radiometer	Room Temperature/ 0.15 K	Hybrid Module	1050 mW	Wearable Devices
[10]	13 GHz	Total Power	1100 K/ 1.4 K	Full Receiver	N.A. (much power)	Fire Detection
[11]	N.A.	Total Power	N.A./ N.A.	Only IF stage	2.2 mW (only IF)	Any Applications
[13]	100 GHz	Total Power	Room Temperature/ 0.43 K	Full receiver	196 mW	Earth Science
This work	Dual Band (1.35/2.75 GHz)	Dicke Radiometer (integrated calibration)	Room Temperature/ 0.9 K (1.35 GHz)	Full receiver Cal. Circuit	52 mW	Body temperature measurement

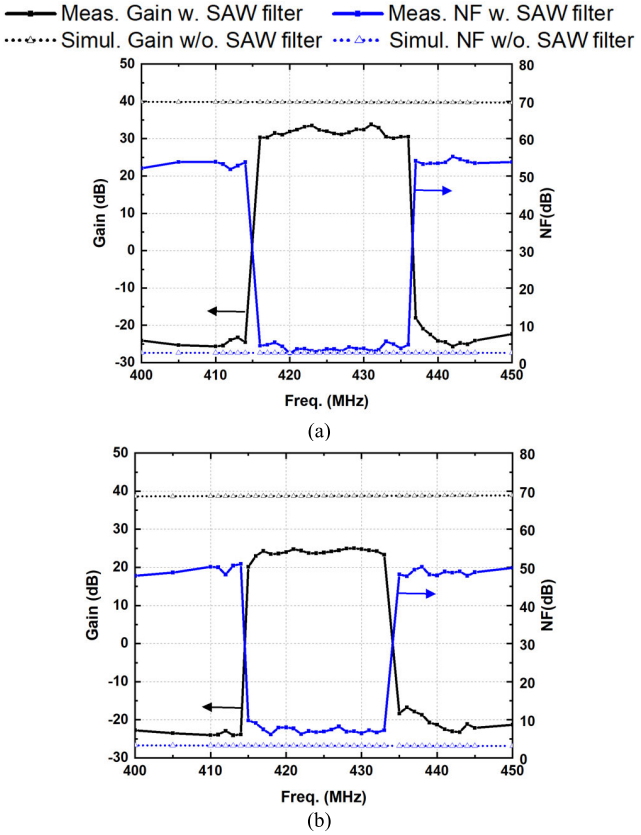

FIGURE 9. Simulated (without SAW filter) and measured Gain (with SAW filter) and Noise Figure (NF) (a) 1.35 GHz band and (b) 2.75 GHz band.

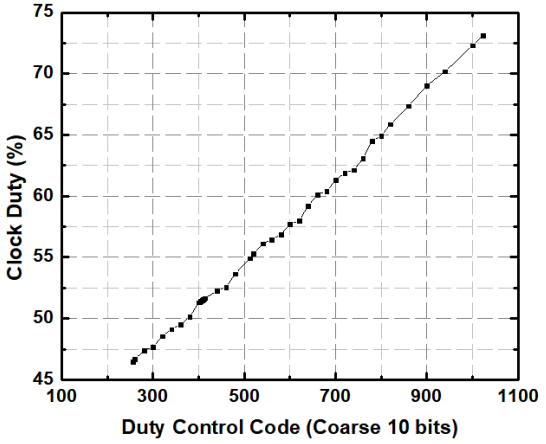

FIGURE 10. Measured clock duty vs. duty control code (0.0356 %).

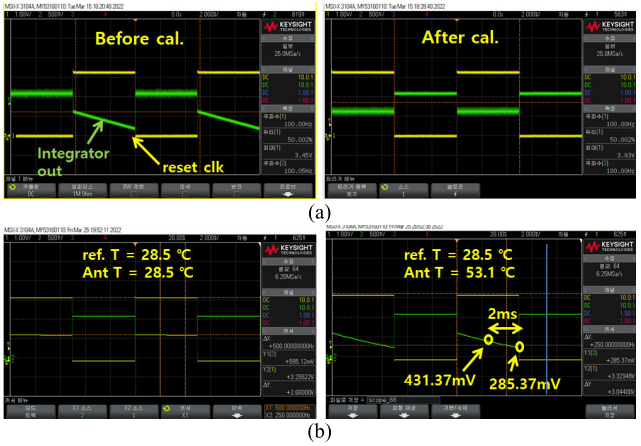

FIGURE 11. Integrator output after calibration (a) and actual measurement of antenna port (b) for 1.35 GHz band.

Fig. 11 (a) shows how the integrator output voltage reaches zero after the calibration of each band in measurement. The clock frequency for the Dicke RF switch and modulator is 1 MHz and the integration time is 5 ms with the 100 Hz clock. For the integration, the off-chip capacitor is used for tuning and its value is 10 nF. In the actual experiment, an external 12 dB LNA module was added at the receiver input for the additive gain and SNR improvement of the receiver.

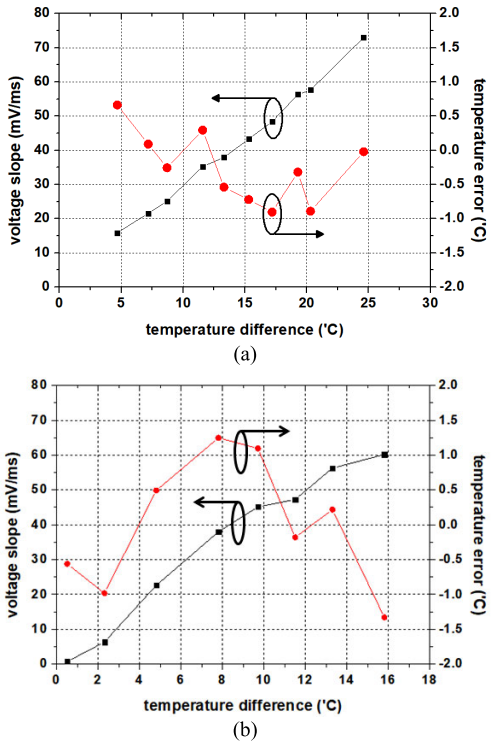

FIGURE 12. Measured voltage slope and temperature error (a) 1.35 GHz band and (b) 2.75 GHz band.

In the calibration procedure, the duty of the clock was initially set to 50 %, and the integrator output voltage increases or declines. By trimming the clock duty with the duty control code, the slope can be diminished, and the calibration is completed when the slope becomes nearly zero. Fig. 11 (b) shows the measured integrator output voltage. Initially, when the target 50 Ω source connected to the antenna port has the same temperature of 28.5 °C as the reference source, no voltage change occurs at the integrator output. However, when the temperature of the target board increases with the heating device on the board, the voltage slope of the integrator output decreases or increases. The temperature difference is 24.6 °C and the integrated voltage is 146 mV after 2 ms. Hence, the measured voltage slope is 2.97 mV/ms • °C. Similarly, the measured integrator outputs after the calibration procedure and temperature difference measurements are performed.

In our IC configuration, the output voltage is converted into a negative voltage if the test port temperature (TREF2 or TANT) is higher than the reference temperature (TREF1). Since the slope changes in proportion to the temperature difference, the temperature error of the proposed Dicke radiometer was found to be less than 0.9 °C by comparing with the actual temperature sensor on the board, as shown in Fig. 12 (a) in the 1.35 GHz band. In the 2.75 GHz band the error is less than 1.3 °C as shown in Fig. 12 (b). Measured average resolution of proposed highly integrated radiometer is 2.86 mV/ms°C and 3.81 mV/ms°C mV/ms°C at 1.35 GHz and 2.75 GHz band.

The performances of the dual band radiometer are summarized in Table. 1. Most earlier studies show the low IC-integration level of the radiometer, which leads to the large form-factor and the high power consumption. However, our proposed design has a much higher level of integration than previous works and also includes the calibration circuits such as duty calibrator, which leads to ease the calibration step only by the digital programming via SPI interface. And they result in low power consumption, small module size, and easy calibration.

IV. CONCLUSION

This study presented the design and development of a highly integrated dual band Dicke radiometer IC that enables accurate temperature sensing insensitive to the receiver gain fluctuation when compared with the total power radiometer. To choose the RF band with only a few microwave interferences, the dual band receiver was designed for 1.35 GHz and 2.75 GHz, providing stable wireless communication. Further, the proposed duty cycle modulator and receiver architecture can achieve calibration effectively, and a temperature error less than 0.9°C was obtained at room temperature. The implemented Dicke radiometer IC also allows small and low-power remote temperature sensors for various applications, such as core body temperature measurement.

ACKNOWLEDGMENT

(Ikhwan Kim and Wonil Jang contributed equally to this work.)

REFERENCES

[1] F. T. Ulaby and D. G. Long, "Thermal radiation," in *Microwave Radar and Radiometric Remote Sensing*. East Lansing, MI, USA: Univ. Michigan Press, 2014, ch. 6, sec. 6, pp. 227–231.

[2] J.-Y. Lefrant, L. Müller, J. E. de La Coussaye, M. Benbabaali, C. Lebris, N. Zeitoun, C. Mari, G. Saïssi, J. Ripart, and J.-J. Eledjam, "Temperature measurement in intensive care patients: Comparison of urinary bladder, oesophageal, rectal, axillary, and inguinal methods versus pulmonary artery core method," *Intensive Care Med.*, vol. 29, no. 3, pp. 414–418, Mar. 2003, doi: 10.1007/s00134-002-1619-5.

[3] O. Uleberg, S. Eidstuen, G. Vangberg, and E. Skogvoll, "Temperature measurements in trauma patients: Is the ear the key to the core?" *Scandin. J. Trauma, Resuscitation Emergency Med.*, vol. 23, no. 1, p. 101, Dec. 2015, doi: 10.1186/s13049-015-0178-z.

[4] J. Lee, G. S. Botello, R. Streeter, and Z. Popovic, "Noninvasive internal body thermometry with on-chip GaAs Dicke radiometer," *IEEE Microw. Wireless Technol. Lett.*, vol. 33, no. 6, pp. 927–930, Jun. 2023, doi: 10.1109/LMWT.2023.3265806.

[5] R. Streeter, G. S. Botello, K. Hall, and Z. Popovic, "Correlation radiometry for subcutaneous temperature measurements," *IEEE J. Electromagn., RF Microw. Med. Biol.*, vol. 6, no. 2, pp. 230–237, Jun. 2022, doi: 10.1109/JERM.2021.3120320.

[6] P. Momenroodaki, W. Haines, M. Fromandi, and Z. Popovic, "Noninvasive internal body temperature tracking with near-field microwave radiometry," *IEEE Trans. Microw. Theory Techn.*, vol. 66, no. 5, pp. 2535–2545, May 2018, doi: 10.1109/TMTT.2017.2776952.

[7] I. Kim, D.-M. Lee, M.-H. Cho, Y.-J. Lee, J.-H. Han, J.-W. Shin, H.-Y. Lee, E.-S. Kim, and N.-Y. Kim, "Compact dual-band on-body near field antenna with reflector for measuring deep core temperature," *IEEE Access*, vol. 11, pp. 32944–32953, 2023, doi: 10.1109/ACCESS.2023.3262997.

[8] I. Kim, D.-M. Lee, Y.-J. Lee, J.-W. Shin, E.-S. Kim, H. Lee, and N.-Y. Kim, "Dual-band on-body near field antenna for measuring deep core temperature with a microwave radiometer," *IEEE Access*, vol. 10, pp. 63715–63722, 2022, doi: 10.1109/ACCESS.2022.3183223.
[9] P. Momenroodaki, Z. Popovic, and R. Scheeler, "A 1.4-GHz radiometer for internal body temperature measurements," in *Proc. Eur. Microw. Conf. (EuMC)*, Sep. 2015, pp. 694–697.
[10] F. Alimenti, L. Roselli, and S. Bonafoni, "Microwave radiometers for fire detection in trains: Theory and feasibility study," *Sensors*, vol. 16, no. 6, p. 906, Jun. 2016, doi: 10.3390/s16060906.
[11] S. G. Vesnin, M. K. Sedankin, L. M. Ovchinnikov, A. G. Gudkov, V. Y. Leushin, I. A. Sidorov, and I. I. Goryanin, "Portable microwave radiometer for wearable devices," *Sens. Actuators A, Phys.*, vol. 318, Feb. 2021, Art. no. 112506, doi: 10.1016/j.sna.2020.112506.
[12] G. Tasselli, F. Alimenti, A. Fonte, D. Zito, L. Roselli, D. De Rossi, A. Lanata, B. Neri, and A. Tognetti, "Wearable microwave radiometers for remote fire detection: System-on-chip (SoC) design and proof of the concept," in *Proc. 30th Annu. Int. Conf. IEEE Eng. Med. Biol. Soc.*, Aug. 2008, pp. 981–984.
[13] F. Alimenti, S. Leone, G. Tasselli, V. Palazzari, L. Roselli, and D. Zito, "IF amplifier section in 90 nm CMOS technology for SoC microwave radiometers," *IEEE Microw. Wireless Compon. Lett.*, vol. 19, no. 11, pp. 731–733, Nov. 2009, doi: 10.1109/LMWC.2009.2032018.
[14] M. Borgarino, A. Polemi, and A. Mazzanti, "Low-cost integrated microwave radiometer front-end for industrial applications," *IEEE Trans. Microw. Theory Techn.*, vol. 57, no. 12, pp. 3011–3018, Dec. 2009, doi: 10.1109/TMTT.2009.2034209.
[15] A. J. Tang, Y. Kim, and Q. J. Gu, "A 0.43K-noise-equivalent-ΔT 100 GHz dicke-free radiometer with 100% time efficiency in 65 nm CMOS," in *IEEE Int. Solid-State Circuits Conf. (ISSCC) Dig. Tech. Papers*, Jan. 2016, pp. 430–431.
[16] A. Tang, T. Reck, R. Shu, L. Samoska, Y. Kim, Y. Ye, Q. Gu, B. J. Drouin, J. Truettel, R. Al Hadi, Y. Xu, S. Sarkozy, R. Lai, M. F. Chang, and I. Mehdi, "A W-band 65 nm CMOS/InP-hybrid radiometer & passive imager," in *IEEE MTT-S Int. Microw. Symp. Dig.*, May 2016, pp. 1–3, doi: 10.1109/MWSYM.2016.7540357.
[17] L. Aluigi, D. Pepe, F. Alimenti and D. Zito, "K-band sige system-on-chip radiometric receiver for remote sensing of the atmosphere," *IEEE Trans. Circuits Syst. I, Reg. Papers*, vol. 64, no. 12, pp. 3025–3035, Dec. 2017, doi: 10.1109/TCSI.2017.2761703.
[18] A. Camps and J. M. Tarongí, "Microwave radiometer resolution optimization using variable observation times," *Remote Sens.*, vol. 2, no. 7, pp. 1826–1843, Jul. 2010, doi: 10.3390/rs2071826.
[19] A. Camps, I. Corbella, J. Bara, and F. Torres, "Radiometric sensitivity computation in aperture synthesis interferometric radiometry," *IEEE Trans. Geosci. Remote Sens.*, vol. 36, no. 2, pp. 680–685, Mar. 1998.
[20] J. W. Hand, G. M. J. V. Leeuwen, S. Mizushina, J. B. V. D. Kamer, K. Maruyama, T. Sugiura, D. V. Azzopardi, and A. D. Edwards, "Monitoring of deep brain temperature in infants using multi-frequency microwave radiometry and thermal modelling," *Phys. Med. Biol.*, vol. 46, no. 7, pp. 1885–1903, Jul. 2001.
[21] S. G. Vesnin, M. K. Sedankin, L. M. Ovchinnikov, A. G. Gudkov, V. Y. Leushin, I. A. Sidorov, and I. I. Goryanin, "Portable microwave radiometer for wearable devices," *Sens. Actuators A, Phys.*, vol. 318, Feb. 2021, Art. no. 112506, doi: 10.1016/j.sna.2020.112506.

IKHWAN KIM was born in Seoul, South Korea, in 1997. He received the B.S. and M.S. degrees in electronic convergence engineering from the Antenna System Laboratory, Kwangwoon University, Seoul, in 2020 and 2022, respectively. He is currently pursuing the Ph.D. degree with the RFIC Laboratory, Department of Electronic Engineering, Kwangwoon University. His current research interests include array antenna, MIMO antenna, broadband antenna, wireless communication antenna, satellite communication antenna, and on-body antenna. He received the Best Student Paper Award at the 2023 IEEE ICEICT.

WONIL JANG received the B.S. and Ph.D. degrees in electronics engineering from Kwangwoon University, South Korea, in 2013 and 2019, respectively. He is currently a Senior Researcher with Silicon Research and Development. His current research interests include low-power RF transceiver SoC used in communication, radar, and sensors.

HYEON-SIK HWANG was born in Seoul, South Korea, in 1997. He received the B.S. degree in computer science from Kwangwoon University, Seoul, in 2020, where he is currently pursuing the integrated M.S. and Ph.D. degree with the RFIC Laboratory, Department of Electronic Engineering. His current research interests include humidity sensors, passive electronic chips for biosensing applications, and neuroscience.

BYEONG-JAE SEO received the B.S. and M.S. degrees in electronic engineering from Kwangwoon University, Seoul, South Korea, in 2017 and 2019, respectively, where he is currently pursuing the Ph.D. degree. His current research interests include CMOS RF/analog IC design for wireless communication systems and UWB radar transceivers.

DONG-MIN LEE was born in Seoul, South Korea, in 1998. He received the B.S. degree from the Department of Computer Science, Kwangwoon University, Seoul, in 2019. He is currently pursuing the integrated M.S. and Ph.D. degree from the RFIC Laboratory, Department of Electronic Engineering, Kwangwoon University. His current research interests include bio-matched antenna, on-body antenna, meta-surface antenna, and array antenna.

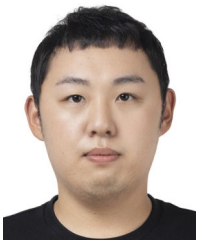

JI-HO HAN received the Ph.D. degree in biomedical engineering from Yonsei University, South Korea, in 2021. He is currently with Easytem Company Ltd., as a Senior Researcher. His current research interests include deep learning from medical data, biomedical signal processing, and transformation drug delivery (TDD).

JAE-WOO SHIN received the M.S. and Ph.D. degrees in biomedical engineering from Yonsei University, South Korea, in 1999 and 2006, respectively. He is currently a CTO with EasyTem Company Ltd. He has developed more than 30 healthcare devices and systems. His current research interests include biomedical signal processing, biomedical instrumentation, arc plasma stimulation of skin effect, transformation drug delivery (TDD), and medical informatics.

YOUNG-RO YOON was born in Seoul, South Korea, in 1957. He received the Ph.D. degree in electronic engineering from Purdue University, Indianapolis, IN, USA. He started his research with the U.S. Naval Research Laboratory, in 1992. After completing his research there, he joined the Department of Biomedical Engineering, Yonsei University, Wonju, as a Professor, in 1994. He is currently a Policy Advisor with the Ministry of Food and Drug Safety, South Korea. He is also a Professor Emeritus with Easytem Company Ltd. His current research interests include bio-signal processing, pattern recognition, and regulatory affairs for medical devices.

TAEHYOUN OH received the B.S. and M.S. degrees in electrical engineering from Seoul National University, in 2005 and 2007, respectively, and the Ph.D. degree in electrical engineering from the University of Minnesota, Minneapolis, under the supervision of Dr. Ramesh Harjani. His doctoral research is focused on high-speed I/O circuits and architectures. In Summer 2010, he worked on I/O channel modeling with the AMD Boston Design Center, MA, USA. In Fall 2011, he worked on I/O architecture and jitter budgeting of the link with Intel Corporation, CA, USA. Since Fall 2012, he has been with the IBM System Technology Group, NY, USA, where he worked on performance verification of high-speed decision feedback equalizer for server processors. Since Spring 2013, he has been with the Department of Electronic Engineering, Kwangwoon University, Seoul, South Korea, as an Assistant Professor. His current research interest includes clock generation IC design.

HYUNG-CHUL PARK received the B.S., M.S., and Ph.D. degrees in electrical engineering from the Korea Advanced Institute of Science and Technology, Daejeon, Republic of Korea, in 1996, 1998, and 2003, respectively. From 2003 to 2005, he was a SoC Design Engineer with Hynix Semiconductor, Seoul, Republic of Korea. From 2005 to 2010, he was an Assistant Professor with Hanbat National University, Daejeon. In 2010, he joined the Department of Electronic and IT Media Engineering, Seoul National University of Science and Technology, Seoul, where he is currently a Professor. His current research interests include wireless modulation/demodulation algorithms, system design/implementation, and interface study between RF/IF stages and digital signal processing.

EUN-SEONG KIM was born in Seoul, South Korea, in 1994. He received the M.S. and Ph.D. degrees in electronic engineering and the M.S. (M.B.A.) degree in biomedical from Kwangwoon University, Seoul, in 2019 and 2021, respectively, and the M.S. degree in clinical pharmacy from Aju University. He is currently a Senior Researcher with Wavepia Company Ltd., and a Research Consultant with the RFIC Laboratory, Kwangwoon University. He has published 62 articles and 25 patents. His current research interests include the fabrication of integrated passive devices, humidity sensors, and flexible printing methods for sensor and RF biosensor and RF cancer treatment applications.

YUN-SEONG EO (Member, IEEE) received the B.S., M.S., and Ph.D. degrees from the Korea Advanced Institute of Science and Technology, Daejeon, South Korea, in 1993, 1995, and 2001, respectively. From 2000 to 2002, he was with the LG Electronics Institute of Technology, Seoul, South Korea, where he was involved in designing RF-integrated circuits (RFICs), such as VCOs, LNAs, and power amplifiers (PAs) using InGaP HBT devices. In 2002, he joined the Samsung Advanced Institute of Technology, Suwon, South Korea, where he developed 5-GHz CMOS PAs and RF transceivers, the development of 900-MHz RF identification (RFID), and 2.4-GHz ZigBee RF transceivers. In 2005, he joined Kwangwoon University, Seoul, where he developed many CMOS RF transceiver ICs for various applications, such as WPAN UWB/ZigBee, DMB, DVB-H, WiFi, and cognitive radio. In 2009, he founded Silicon Research and Development Inc., Seongnam, South Korea, where he developed CMOS-based UWB RF transceivers and radar chips. He is currently a Professor with the Electronics Engineering Department, Kwangwoon University. His current interests include UWB radar and FMCW radar ICs for various sensor applications.

NAM-YOUNG KIM was born in Seoul, South Korea. He received the M.S. degree in clinical pharmacy from Aju University, the Ph.D. degree in electronic engineering from The State University of New York (SUNY) at Buffalo, and the Ph.D. degree in theology from Midwest University. He was a Research Scientist with CEEM, SUNY at Buffalo, in 1994. Then, he joined the Department of Electronic Engineering, Kwangwoon University, as a Professor, in 1995. As the Founder of the RFIC Center, he was the Director of the Fusion Technology Center of RF and Bio-Related Research. He has published 295 journals and 405 conference papers, 33 books, and registered 245 patents. His current research interests include RF semiconductor devices, RFICs and MMICs, RF biosensors, and RF applications in cancer medical treatment.